

Article

A Fluorescence Inner-Filter Effect Based Sensing Platform for Turn-On Detection of Glutathione in Human Serum

Shurong Tang ^{*,†}, Xiuhua You [†], Quanhui Fang, Xin Li, Guangwen Li, Jinghua Chen and Wei Chen 

Department of Pharmaceutical Analysis, Faculty of Pharmacy, Fujian Medical University, Fuzhou 350108, China; hhyou4906@163.com (X.Y.); 18250485385@163.com (Q.F.); lx281032@163.com (X.L.); lgw6301@fjmu.edu.cn (G.L.); cjh_huaxue@126.com (J.C.); chenandhu@163.com (W.C.)

* Correspondence: srtang@fjmu.edu.cn; Tel.: +86-591-2286-273

† These authors contributed equally to this work.

Received: 23 November 2018; Accepted: 2 January 2019; Published: 9 January 2019



Abstract: A novel turn-on fluorescence assay was developed for the rapid detection of glutathione (GSH) based on the inner-filter effect (IFE) and redox reaction. Molybdenum disulfide quantum dots (MoS₂ QDs), which have stable fluorescent properties, were synthesized with hydrothermal method. Manganese dioxide nanosheets (MnO₂ NSs) were prepared by exfoliating the bulk δ -MnO₂ material in bovine serum albumin (BSA) aqueous solution. The morphology structures of the prepared nanoparticles were characterized by transmission electron microscope (TEM). Studies have shown that the fluorescence of MoS₂ QDs could be quenched in the presence of MnO₂ NSs as a result of the IFE, and is recovered after the addition of GSH to dissolve the MnO₂ NSs. The fluorescence intensity showed a good linear relationship with the GSH concentration in the range 20–2500 μ M, the limit of detection was 1.0 μ M. The detection method was applied to the analysis of GSH in human serum samples. This simple, rapid, and cost-effective method has great potential in analyzing GSH and in disease diagnosis.

Keywords: fluorescence inner-filter effect; manganese dioxide nanosheets; molybdenum disulfide quantum dots; glutathione detection; human serum

1. Introduction

Glutathione (GSH), the most abundant intracellular low-molecular-weight biothiol, is a tripeptide consisting of cysteine, glutamic acid, and glycine. As an essential endogenous antioxidant, GSH plays crucial roles in biological systems and many cellular processes, such as maintaining the appropriate intracellular redox status, protecting against many toxins, and promoting metabolism [1]. Abnormal GSH levels in the blood are closely related with some clinical diseases including leucocyte loss, inflammation, liver damage, psoriasis, Parkinson's, Alzheimer's, and cancer [2,3]. It has been found that the GSH level is significantly elevated in cancer cells [4]. Therefore, developing a simple and sensitive method for GSH detection in human serum is critically important for understanding GSH homeostasis in clinical settings and in effective cancer diagnosis at an early stage.

To date, a number of analytical methods have been established for GSH measurement, including high-performance liquid chromatography [5], mass spectrometry [6], surface enhanced Raman scattering [7], enzyme-linked immunosorbent assay [8], electrochemical analysis [9], and fluorescence spectroscopy [10]. Fluorescence spectrometry has been found to be a powerful tool for GSH detection because of its simplicity, high sensitivity, good flexibility, and nondestructive readout [11,12]. Several fluorescence assays have been developed for estimating GSH levels in biological samples [13,14]. Most

of these assays are based on fluorescence “turn-off” patterns or organic dye probes, which make them susceptible to false positive results, lowered sensitivity, or poor photostability. Thus, we still need to establish a novel fluorescence “turn-on” method for the sensing of GSH.

Owing to the exceptional advantages, fluorescent nanomaterials have recently gained great attention as promising substitutes for organic dyes, such as quantum dots [15,16], gold nanoclusters [17,18], carbon dots [19,20], and upconversion nanoparticles [21]. Among them, quantum dots (QDs), which display superior properties including a high-fluorescence quantum yield, size/composition-dependent tunable luminescence, broad excitation/narrow emission spectrum, excellent stability, and good resistance to photobleaching [22], have become ideal probes for signal transduction in the fluorescent assays. For instance, CdSe@ZnS QDs have been used to construct a fluorescence lateral flow biosensor for the rapid detection of GSH [16]. Crystal violet-functionalized CdTe QDs were synthesized for detecting GSH in water [23]. Au nanocluster based fluorescent sensor has been designed for turn-on sensing of GSH, in which Hg^{2+} acted as a quencher [24]. The introduction of highly toxic heavy metal ions (Cd^{2+} or Hg^{2+}) into these systems posed a big threat to the environment. MoS_2 QDs, novel fluorescent nanoparticles with ideal environmental compatibility, high fluorescent intensity, easy operability, and a low cost are a promising candidate for GSH analysis [25–27].

Conventional sensing systems based on fluorescence resonance energy transfer (FRET) have been used to detect various analytes. However, they only work when the fluorophore and quencher are at a particular distance, which restrict the application of FRET-based fluorescence assays. The fluorescence inner-filter effect (IFE) refers to the absorption of the excitation/emission light of fluorophores by appropriate absorbers [28]. The sensitivity of the IFE system can be enhanced due to that the fluorescence of fluorophore would be exponentially changed with the absorbance of absorber [29]. MnO_2 nanosheets (NSs), a new class of two-dimensional nanomaterials, have received increasing attention due to their attractive characteristics, including their high specific surface area, broad absorption spectrum (200–600 nm), large extinction coefficient ($9.6 \times 10^3 \text{ M}^{-1} \text{ cm}^{-1}$) [30], unique redox activity, stability, and biocompatibility [31]. These features enable them to be used as a potentially ideal fluorescent absorber in the IFE-based assay.

Herein, we developed a simple “turn-on” fluorescence assay for the rapid detection of GSH based on the IFE. In this system, MoS_2 QDs were used as the fluorophore and MnO_2 NSs as the absorber. The existence of GSH can cause the decomposition of MnO_2 NSs, leading to a concentration-dependent reduction of MnO_2 and proportional increase of the fluorescence. This assay can be conveniently used for the sensing of GSH in human blood serum, which holds great promise for biomedical applications.

2. Materials and Methods

2.1. Materials and Instruments

Hydrogen peroxide (H_2O_2) was purchased from Hengxing Chemical Reagent Co., Ltd. (Tianjin, China). Sodium molybdate dihydrate ($\text{Na}_2\text{MoO}_4 \cdot 2\text{H}_2\text{O}$) was purchased from Phygene Biotechnology Co., Ltd. (Fuzhou, China). Manganese sulfate monohydrate ($\text{MnSO}_4 \cdot \text{H}_2\text{O}$), magnesium chloride hexahydrate ($\text{MgCl}_2 \cdot 6\text{H}_2\text{O}$), sodium chloride (NaCl), calcium chloride (CaCl_2), copper sulfate (CuSO_4), and hydrochloric acid (HCl) were purchased from the Sinopharm Chemical Reagent Co., Ltd. (Shanghai, China). Bovine serum albumin (BSA), tetramethylammonium hydroxide (TMA·OH), glutathione (GSH), oxidized glutathione (GSSG), L-glutamate (L-Glu), L-histidine (L-His), L-phenylalanine (L-Phe), glycine (Gly), cystine (3,3'-Dith), L-methionine (L-Met), and DL- α -aminopropionic acid (DL- α -Ala) were purchased from Aladdin Reagent Company (Shanghai, China). The reagents used were all analytical grade. Human serum was kindly provided by the Hospital of Fujian Medical University. Deionized water was prepared by Milli-Q Water Purification System for all the experiments.

The absorption spectra were conducted on a UV-2600 UV-vis spectrophotometer (Shimadzu, Tokyo, Japan). Fluorescence spectrum was recorded on an F-4600 fluorescence spectrophotometer

(Hitachi, Tokyo, Japan). High-resolution transmission electron microscopic (HRTEM) imaging was performed on a JEOL 2100F field emission transmission electron microscope (JEOL, Tokyo, Japan). The dynamic light scattering (DLS) experiment was performed on a Zetasizer Nano-ZS90 (Malvern, Worcestershire, UK). The XRD pattern was obtained by a D8 Advance X-ray diffractometer (Bruker, Karlsruhe, Germany). Absolute fluorescence quantum yields (QY) measurements were conducted on an Edinburgh FLS 980 spectrometer with an integrating sphere (Edinburgh, Livingston, UK).

2.2. Preparation of Bulk δ -MnO₂ and MnO₂ NSs

Bulk δ -MnO₂ was prepared as reported previously [32]. Typically, 20 mL of a mixture containing TMA·OH (0.6 M) and H₂O₂ (3 wt %) was added into 10 mL of MnSO₄ (0.3 M) aqueous solution within 15 s. The as-prepared dark brown solution was stirred vigorously overnight at room temperature. Then, the resulting precipitate was removed by centrifugation at 10,000 rpm for 10 min, and washed three times with ultrapure water. Finally, the precipitate was dried in a vacuum oven at 30 °C.

The MnO₂ NSs were prepared by exfoliating the bulk δ -MnO₂ in BSA aqueous solution [33]. Briefly, 10 mg bulk δ -MnO₂ was added into a 10 mL BSA (1 mg/mL) aqueous solution and the mixture was sonicated for 12 h. Then, the suspension was centrifuged at 1000 rpm for 20 min to remove the unexfoliated MnO₂. The supernatant, which contained the MnO₂ NSs, was collected and stored in a refrigerator at 4 °C.

2.3. Preparation of MoS₂ QDs

MoS₂ QDs were synthesized by a hydrothermal method according to the literature [34] with some modifications. Concisely, 0.25 g of Na₂MoO₄·2H₂O was dissolved in 25 mL of water and subjected to ultrasonication for 5 min. Then, the solution was adjusted to pH 6.5 with 0.1 M HCl. After that, 0.5 g Cys and 50 mL water were added into the solution followed by ultrasonication for 10 min. The mixture was then heated in a Teflon-lined stainless steel autoclave at 200 °C for 36 h. After cooling to room temperature, the supernatant was collected after being centrifuged at 12,000 rpm for 30 min. Finally, the stable MoS₂ QDs were obtained after dialyzed for 19 h to remove the impurity using dialysis bag (3500 Da).

2.4. Detection of GSH

Firstly, 5 μ L of GSH aqueous solution with different concentrations was added into 100 μ L of 0.2 M acetate buffer (pH = 5.0) in a low adsorption tube. Then, 15 μ L of MnO₂ NSs (1.0 mM) was added and the mixture was shaken and reacted for 10 min. Next, 80 μ L of MoS₂ QDs (1.6 mg/mL) was added into the as-prepared solution, shaking well to ensure complete reaction. Finally, the fluorescence intensity of the whole reaction solution was detected at room temperature (Ex: 320 nm, Em: 340–600 nm, the peak was about 400 nm). The specific experiments were conducted in the same way, except using other amino acid instead of GSH solution.

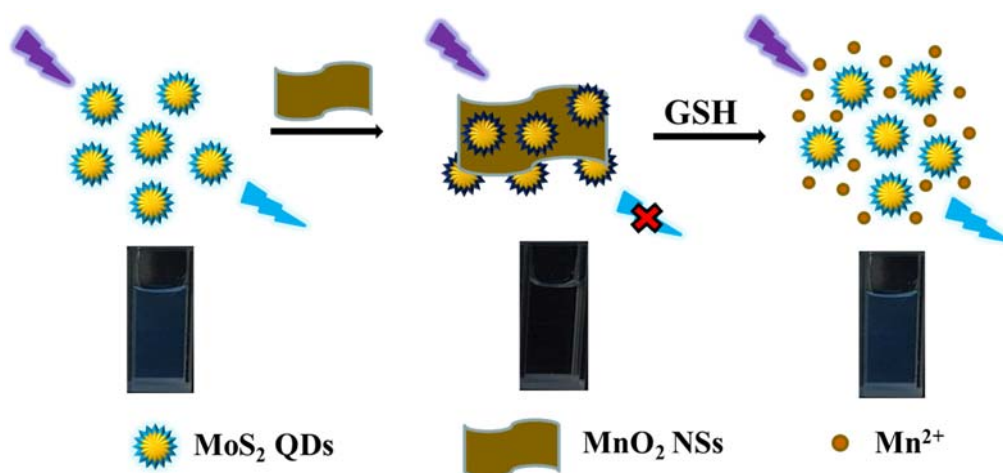
2.5. Analysis of GSH in Human Serum Samples

The standard addition method was used to analyze the GSH level in human serum. Briefly, 95 μ L of 0.2 M acetate buffer (pH = 5.0), 5 μ L different concentrations of GSH aqueous solution, 5 μ L human serum, and 15 μ L of MnO₂ NSs were added into a low-adsorption tube. After being reacted for 10 min, 80 μ L of MoS₂ QDs was added into the above mixture, shaking well to ensure complete reaction. Finally, the fluorescence intensity of the resulting solution was measured. The whole process was carried out at room temperature.

3. Results and Discussion

3.1. Fluorescence Sensing Principle of GSH

The sensing principle of GSH is shown in Scheme 1. The synthesized MoS₂ QDs emitted blue fluorescence under irradiation at 320 nm. MnO₂ NSs possessed a broad absorption spectrum and large molar extinction coefficient, making them a promising quencher in the IFE. After the addition of MnO₂ NSs, the fluorescence of MoS₂ QDs was effectively quenched as a result of the IFE. In the presence of reductive GSH, the MnO₂ NSs (strong oxidation ability) can be decomposed through the redox reaction. The released Mn²⁺ lost its quenching ability, thus the fluorescence of MoS₂ QDs was recovered. On the basis of this mechanism, a “turn-on” fluorescent detection method was developed for the rapid sensing of GSH in human serum.



Scheme 1. Schematic diagram of the fluorescence assay for GSH detection.

3.2. Characterization of MoS₂ QDs and MnO₂ NSs

The morphologies of MoS₂ QDs and MnO₂ NSs were characterized by transmission electron microscopy (TEM). TEM (Figure 1A) and DLS (Figure 1C) analysis results show that the synthesized MoS₂ QDs are well dispersed with the particle size of about 3 nm. The HRTEM image shows that the MoS₂ QDs has obvious lattice fringes (Figure 1B). Figure 1D is the XRD spectrum of MoS₂ QDs. Three major diffraction peaks attributed to (100), (102), and (103) planes of MoS₂ can be observed [34]. The fluorescence properties of the MoS₂ QDs were further investigated. From Figure 2, it was clearly observed that the most intense peak of MoS₂ QDs appeared at 320 nm in the excitation spectrum (curve a). Under this excitation light, a well distinguishable peak with maximum emission intensity at 400 nm appeared (curve b). The MoS₂ QDs solution emitted blue fluorescence when exposure to a 365 nm UV lamp (inset Figure 2). As shown in Figure 3A, an ultrathin lamellar structure with an irregular edge of MnO₂ NSs was observed. Figure 3B shows the HRTEM image of MnO₂ NSs with the diffraction pattern. The UV-Vis spectrum shows that the prepared MnO₂ NSs possessed a broad absorption in the range 200–600 nm (Figure 3C).

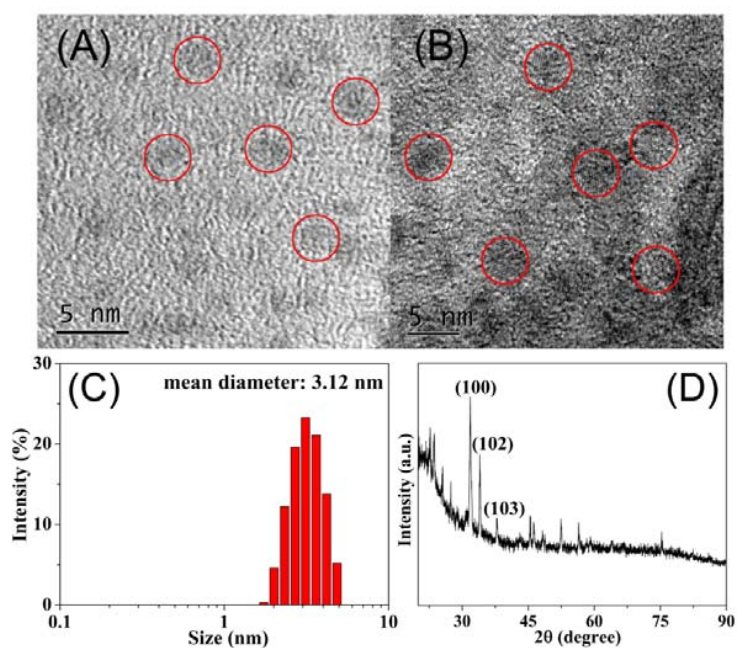


Figure 1. (A) TEM; (B) high-resolution transmission electron microscopic (HRTEM) image; (C) dynamic light scattering (DLS) analysis; and (D) XRD pattern of MoS₂ quantum dots (QDs).

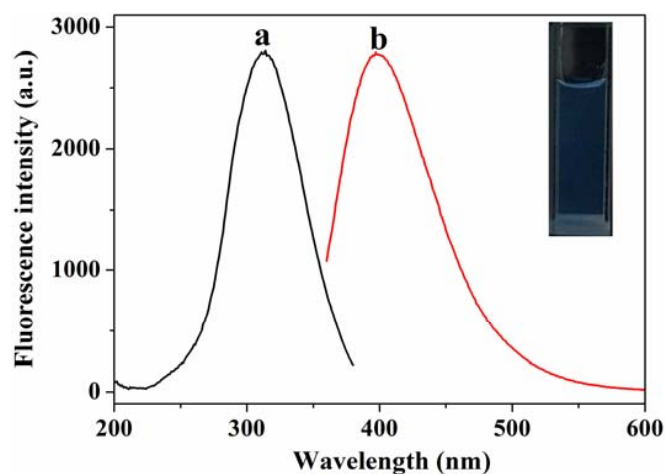


Figure 2. Fluorescence excitation (a) and emission (b) spectra of MoS₂ QDs (Inset: The photo of MoS₂ QDs solution under UV irradiation). Detection parameters: Ex slit, 5.0 nm; Em slit, 10.0 nm; Scan speed, 1200 nm/min; PMT, 700 V.

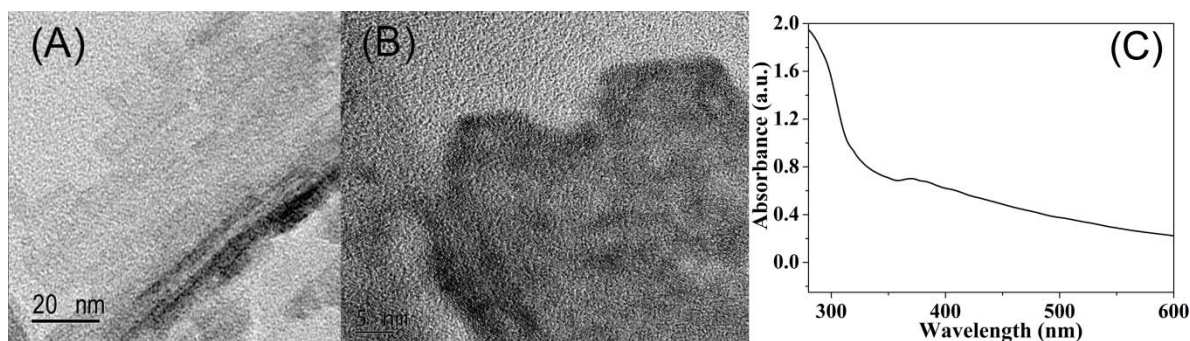


Figure 3. (A) TEM; (B) HRTEM image; and (C) UV-Vis spectrum of manganese dioxide nanosheets (MnO₂ NSs).

3.3. Feasibility Analysis of GSH Detection

To investigate the ability of GSH to dissolve MnO_2 NSs, different concentrations of GSH were added into the MnO_2 NSs, and then the solutions were analyzed by UV-Vis spectrophotometer. As shown in Figure 4, the MnO_2 NSs has a characteristic absorption peak at about 380 nm (curve a), which is consistent with the literature [35]. With the increase of GSH concentration, the absorption intensity decreased (curve b–e) and the color of the solution became gradually shallower (inset Figure 4). These results indicated that the MnO_2 NSs can be decomposed by GSH through the redox reaction [36]. According to the Beer-Lambert law ($A = kbc$, $k = 9.6 \times 10^3 \text{ M}^{-1} \text{ cm}^{-1}$, $b = 1 \text{ cm}$), the concentration of the synthetic MnO_2 NSs was calculated to be about 1 mM.

In order to verify the fluorescence sensing feasibility of GSH based on the probe of MoS_2 QDs and MnO_2 NSs, serials experiments were performed (Figure 5). It can be seen that MoS_2 QDs emitted strong fluorescence (bar graph a). The added GSH did not greatly change the fluorescence intensity of MoS_2 QDs (bar graph b). After addition of MnO_2 NSs, the fluorescence of MoS_2 QDs was significantly quenched (bar graph c). In the presence of GSH, the MnO_2 NSs was dissolved and thus recovered the fluorescence (bar graph d). Therefore, it can be proved that the proposed fluorescence assay was feasible for the “turn-on” detection of GSH. The QY of the MoS_2 QDs probe and for the restored fluorescence in the presence of GSH were measured to be 2.13% and 2.39% by the absolute quantum yield measurement method, respectively.

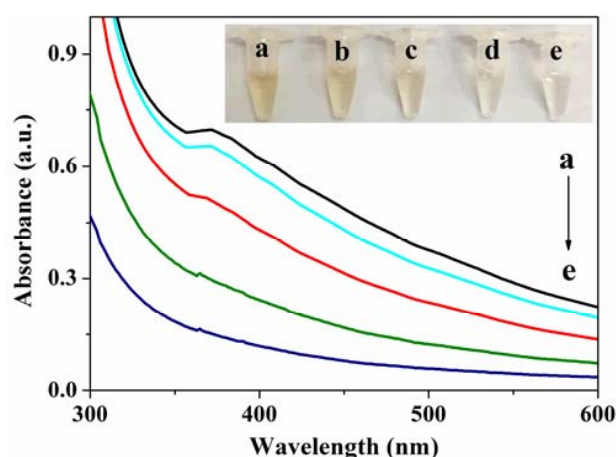


Figure 4. UV-Vis spectra of MnO_2 NSs solution (0.075 mM) after the addition of different concentrations of GSH (a: 0, b: 100, c: 500, d: 2000, e: 5000 μM) (Inset: The corresponding photographs of the above solutions).

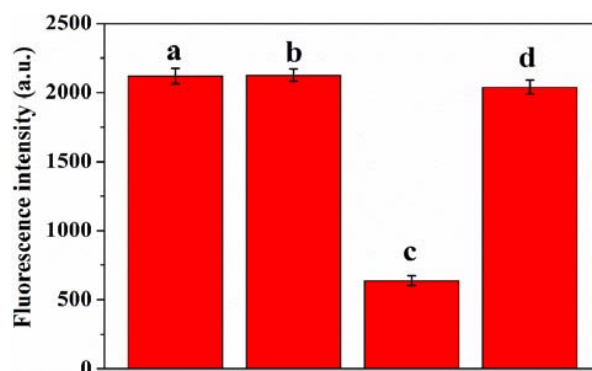


Figure 5. The effect of MnO_2 NSs and glutathione (GSH) on the fluorescence intensity of MoS_2 QDs. (bar graph a: MoS_2 QDs (0.64 mg/mL), bar graph b: MoS_2 QDs + 5 μL 400 mM GSH, bar graph c: MoS_2 QDs + 15 μL 1.0 mM MnO_2 NSs, bar graph d: MoS_2 QDs + 15 μL 1.0 mM MnO_2 NSs + 5 μL 400 mM GSH).

3.4. Optimization of Experimental Conditions

The concentration of MoS₂ QDs and MnO₂ NSs, used as the fluorescence and quencher probe, respectively, have a great effect on the detection sensitivity. The fluorescence intensities of different concentrations of MoS₂ QDs solutions were determined. As shown in Figure 6A, the fluorescence intensity decreased as the dilution multiple of the MoS₂ QDs increased, then the decreasing trend gradually tended to be gentle. Considering the sensitivity and fluorescence intensity, the final concentration of 2.5-fold diluted MoS₂ QDs solution was used in the following experiments. As the amount of MnO₂ NSs increased, the fluorescence of MoS₂ QDs sharply decreased (Figure 6B). Excessive MnO₂ NSs reduces the GSH detection sensitivity. After a comprehensive analysis of the fluorescence inhibition degree and sensitivity, 15 µL of MnO₂ NSs was finally selected. The reaction time between GSH and MnO₂ NSs was also investigated. The fluorescence intensity increased gradually with the time prolonging from 0 to 10 min, then it tended to be stable (Figure 6C). Therefore, the reaction time was selected to be 10 min.

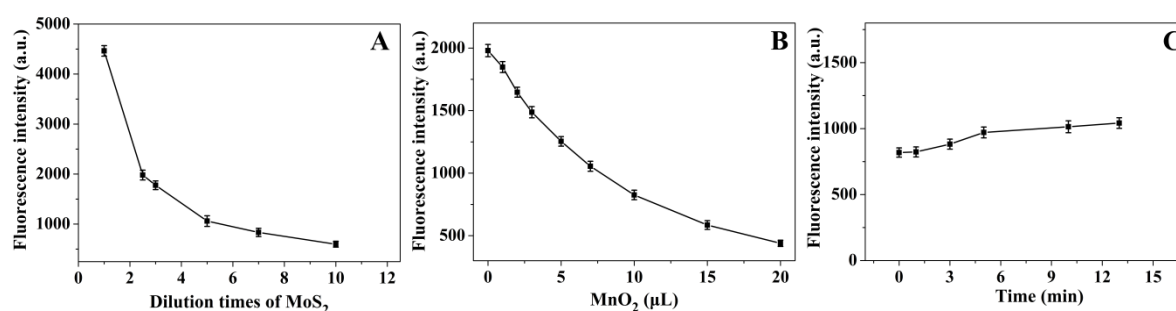


Figure 6. (A) The effect of MoS₂ QDs dilution time (initial concentration 1.6 mg/mL); (B) MnO₂ NSs concentration (1.0 mM); (C) and the reaction time between GSH and MnO₂ NSs on the fluorescence intensity.

3.5. GSH Detection Sensitivity

To investigate the capability of the fluorescence assay for quantitative measurement of GSH, different concentrations of GSH were added to the system and the fluorescence responses were recorded under optimal conditions. The fluorescence of MoS₂ QDs was found to be gradually restored with an increasing concentration of GSH (Figure 7A). The more GSH added, the more MnO₂ NSs decomposition, which resulted in a restoration of the fluorescence. The standard curve was obtained between the fluorescence intensity and the GSH concentration (Figure 7B). The inset in Figure 7B shows that the fluorescence intensity was linearly related to the GSH concentration in a range from 0.02 to 2.5 mM with a correlation coefficient of 0.996. The linear equation is $Y = 301.94X + 702.72$, where Y is the fluorescence intensity and X is the concentration of GSH (mM). The detection limit was calculated to be 1.0 µM according to the three-fold standard deviation of the blank signal (3σ). As shown in Table 1, the detection sensitivity was comparable to that of some reported methods and could meet the requirement of GSH detection in biological and clinical applications (mM levels) [7].

Table 1. Comparison of our present work with other methods for GSH detection.

| Methods | Probes | Linear Range | LOD | References |
|------------------|---|--------------|---------|------------|
| Fluorescence | MnO ₂ -UCNPs | - | 0.9 µM | [36] |
| Fluorescence | CdSe@ZnS QDs-MnO ₂ | 0.05~1.5 mM | 16.3 µM | [16] |
| Fluorescence | CDs-MnO ₂ NPs | 1~200 µM | 0.6 µM | [37] |
| Fluorescence | GQDs-MnO ₂ composite | 1~1000 µM | 0.45 µM | [38] |
| Colorimetric | MnO ₂ NSs-TMB | 1~25 µM | 0.3 µM | [31] |
| Colorimetric | GSH-AuNCs-TMB | 2~25 µM | 0.42 µM | [39] |
| Electrochemistry | CdTe QDs | 24~214 µM | 8.3 µM | [40] |
| Fluorescence | MoS ₂ QDs-MnO ₂ NSs | 20~2500 µM | 1.0 µM | This work |

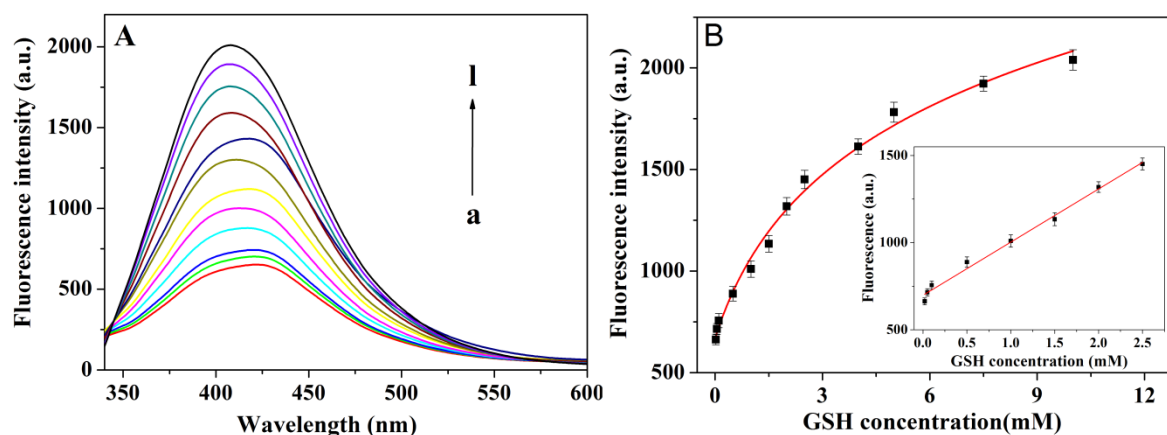


Figure 7. (A) Fluorescence spectra of the system at different GSH concentrations (From a to l: 0.02, 0.05, 0.1, 0.5, 1, 1.5, 2, 2.5, 4, 5, 7.5, and 10 mM; MoS₂ QDs 0.64 mg/mL, MnO₂ NSs 0.075 mM); (B) the relationship between GSH concentration and the fluorescence intensity (Inset: The calibration plot of fluorescence intensity against the concentrations of GSH).

3.6. Interference Detection Results

To assess the selectivity of GSH detection based on the MoS₂ QDs-MnO₂ NSs system, the influence of some amino acids, metal ions, and proteins which possibly exist in human serum was studied. As shown in Figure 8, the system exhibited a remarkable increase in fluorescence in the presence of GSH. On the contrary, there were no obvious changes in fluorescence intensity with the other molecules. It was also found that when GSH was mixed with some other amino acids, the fluorescent intensity was similar to GSH alone. Although a high concentration of cysteine (Cys) and homo-cysteine (H-Cys) can cause a measurable fluorescence response to this system, their contents (μ M levels) are much lower than that of GSH (mM levels) in biological systems [41,42]. These results show that the system displays a highly selective response of fluorescence enhancement towards GSH over other molecules.

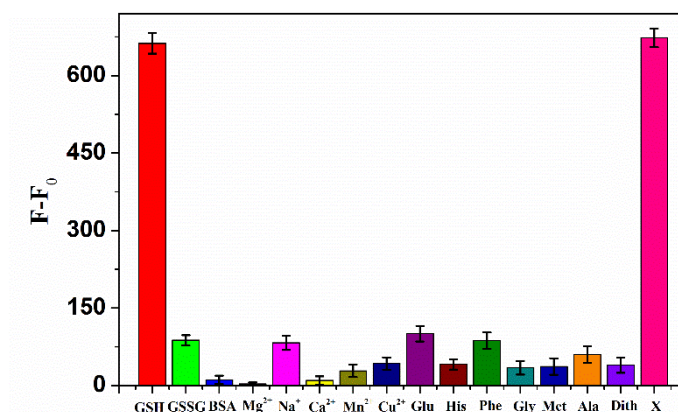


Figure 8. Selectivity investigation of the system for GSH detection. The concentration of GSH, oxidized glutathione (GSSG), and other amino acid solutions were 2 mM, bovine serum albumin (BSA) was 1 mg/mL, and the metal ions concentration was 5 mM. Bar graph “X” was the fluorescent recovery of the mixture of several amino acids (Glu, His, Phe, Gly, Met, Ala, and Dith with a concentration of 2 mM) with 2 mM GSH.

3.7. GSH Detection in Human Serum

Human serum experiments were further performed to investigate the feasibility of the MoS₂ QDs-MnO₂ NSs system in the analysis of GSH in actual samples. Different concentrations of standard GSH were spiked in the human serum and the samples were measured in parallel three times. As shown in Table 2, the recovery rate of the method was found to be 99.2–104%, and the RSD was within

10%. It is shown that this method can be used for the detection of GSH in human serum with acceptable reproducibility and accuracy.

Table 2. Analysis of GSH in human serum samples (n = 3).

| Sample | Add/mM | Found/mM | Recovery/% | RSD/% |
|--------|--------|----------|------------|-------|
| 1 | 0 | 0.193 | - | 9.6 |
| 2 | 0.1 | 0.104 | 104 | 2.1 |
| 3 | 1.0 | 0.992 | 99.2 | 2.6 |

3.8. Reaction Mechanism Discussion

The fluorescence internal filter effect refers to the phenomenon that occurs when the fluorophore coexists with other absorbents, and the fluorescence is weakened due to the absorption of the excitation or emission light by the absorbent. The broad absorption of MnO₂ NSs possesses a peak at about 380 nm (Figure 3C), which overlaps both with the emission and excitation wavelength of MoS₂ QDs. Therefore, when both of them exist in the system, the fluorescence of MoS₂ QDs will be quenched due to the IFE (Figure 9, curve a). Interestingly, we found that after high-speed centrifugation of the reaction solution, the fluorescence of the supernatant was restored (Figure 9, curve b), possibly as a result of the suspended MnO₂ NSs in the solution being separated from the MoS₂ QDs and precipitated in the bottom of the centrifuge tube. Thus, the fluorescence of MoS₂ QDs in the supernatant cannot be quenched by MnO₂ NSs through the IFE. The experimental results confirmed that the detection of GSH was based on the IFE, which is different from the reported FRET mechanism of single-layer MnO₂ nanosheets [36,43].

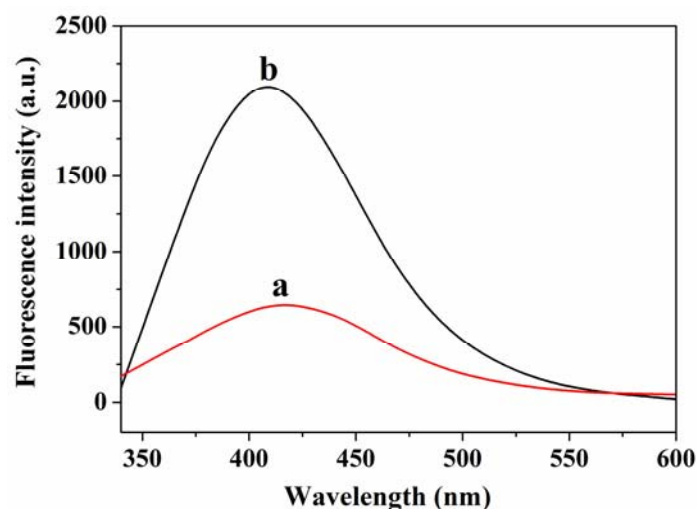


Figure 9. Fluorescence spectra of the solution containing MoS₂ QDs and MnO₂ NSs before (a) or after (b) centrifuge treatment.

3.9. Stability Investigation

The stability of the prepared MoS₂ QDs with and without dialysis was investigated. We found that after being placed at room temperature for 42 days, the synthesized MoS₂ QDs after dialysis retained about 96% of their original fluorescence intensity. However, the fluorescence of MoS₂ QDs decreased sharply without dialysis, being only 61% of the previous measurement. It shows that the stability of MoS₂ QDs is greatly improved by dialysis treatment, which is a benefit for practical applications.

4. Conclusions

In summary, a signal enhanced fluorescence assay was developed for the rapid detection of GSH in human serum. The fluorescence of MoS₂ QDs can be effectively quenched by MnO₂ NSs as a

result of the IFE. Interestingly, the quenched fluorescence was restored when reductive GSH was introduced to dissolve MnO₂ NSs through the redox reaction. The final fluorescence intensity was linearly correlated with the concentration of GSH. The whole detection process can be completed within 15 min. Notably, the fluorescence response was selective toward GSH without interference from other substances in human serum. Thus, the assay was successfully used for the analysis of GSH in human serum samples. We anticipate that this simple, stable, selective, and cost-effective “turn-on” fluorescent assay has a good prospect of application for GSH analysis in biomedical fields.

Author Contributions: S.T. and X.Y. conceived and designed the experiments; Q.F. and X.L. performed the experiments; X.Y. and G.L. have helped analyze the results of the measured data; S.T. wrote the paper. W.C. and J.C. have proposed valuable suggestions on the revise of the manuscript. All coauthors reviewed and revised the paper.

Funding: This research was funded by the National Natural Science Foundation of China (21874019, 21675024), and the Natural Science Foundation of Fujian Province (2017J01575, 2017J07001, 2016J01049, 2016Y9056).

Conflicts of Interest: The authors declare no conflict of interest.

References

1. Forman, H.J.; Zhang, H.; Rinna, A. Glutathione: Overview of its protective roles, measurement, and biosynthesis. *Mol. Asp. Med.* **2009**, *30*, 1–12. [[CrossRef](#)] [[PubMed](#)]
2. Lu, S.C. Regulation of glutathione synthesis. *Mol. Asp. Med.* **2009**, *30*, 42–59. [[CrossRef](#)] [[PubMed](#)]
3. Pocernich, C.B.; Butterfield, D.A. Elevation of glutathione as a therapeutic strategy in Alzheimer disease. *Biochim. Biophys. Acta* **2012**, *1822*, 625–630. [[CrossRef](#)] [[PubMed](#)]
4. Guo, Y.; Wang, H.; Sun, Y.S.; Qu, B. A disulfide bound-molecular beacon as a fluorescent probe for the detection of reduced glutathione and its application in cells. *Chem. Commun.* **2012**, *48*, 3221–3223. [[CrossRef](#)] [[PubMed](#)]
5. Childs, S.; Haroune, N.; Williams, L.; Gronow, M. Determination of cellular glutathione: Glutathione disulfide ratio in prostate cancer cells by high performance liquid chromatography with electrochemical detection. *J. Chromatogr. A* **2016**, *1437*, 67–73. [[CrossRef](#)] [[PubMed](#)]
6. Huang, Y.-F.; Chang, H.-T. Analysis of adenosine triphosphate and glutathione through gold nanoparticles assisted laser desorption/ionization mass spectrometry. *Anal. Chem.* **2007**, *79*, 4852–4859. [[CrossRef](#)]
7. Saha, A.; Jana, N.R. Detection of cellular glutathione and oxidized glutathione using magnetic-plasmonic nanocomposite-based “Turn-Off” surface enhanced raman scattering. *Anal. Chem.* **2013**, *85*, 9221–9228. [[CrossRef](#)]
8. Wawegama, N.K.; Browning, G.F.; Kanci, A.; Marendra, M.S.; Markham, P.F. Development of a recombinant protein-based enzyme-linked immunosorbent assay for diagnosis of Mycoplasma bovis infection in cattle. *Clin. Vaccine Immunol.* **2014**, *21*, 196–202. [[CrossRef](#)]
9. Zhu, W.; Jiang, G.; Xu, L.; Li, B.; Cai, Q.; Jiang, H.; Zhou, X. Facile and controllable one-step fabrication of molecularly imprinted polymer membrane by magnetic field directed self-assembly for electrochemical sensing of glutathione. *Anal. Chim. Acta* **2015**, *886*, 37–47. [[CrossRef](#)]
10. Yoon, S.A.; Kim, W.; Sharma, A.; Verwilt, P.; Won, M.; Lee, M.H. A fluorescent Cy7-mercaptopyridine for the selective detection of glutathione over homocysteine and cysteine. *Sensors* **2018**, *18*, 2897. [[CrossRef](#)]
11. Niu, L.Y.; Guan, Y.S.; Chen, Y.Z.; Wu, L.Z.; Tung, C.H.; Yang, Q.Z. BODIPY-based ratiometric fluorescent sensor for highly selective detection of glutathione over cysteine and homocysteine. *J. Am. Chem. Soc.* **2012**, *134*, 18928–18931. [[CrossRef](#)] [[PubMed](#)]
12. Yuan, L.; Lin, W.; Zheng, K.; Zhu, S. FRET-based small-molecule fluorescent probes: Rational design and bioimaging applications. *Acc. Chem. Res.* **2013**, *46*, 1462–1473. [[CrossRef](#)] [[PubMed](#)]
13. Niu, L.Y.; Chen, Y.Z.; Zheng, H.R.; Wu, L.Z.; Tung, C.H.; Yang, Q.Z. Design strategies of fluorescent probes for selective detection among biothiols. *Chem. Soc. Rev.* **2015**, *44*, 6143–6160. [[CrossRef](#)] [[PubMed](#)]
14. Xu, H.; Hepel, M. “Molecular beacon”-based fluorescent assay for selective detection of glutathione and cysteine. *Anal. Chem.* **2011**, *83*, 813–819. [[CrossRef](#)] [[PubMed](#)]

15. Pan, J.; Zheng, Z.; Yang, J.; Wu, Y.; Lu, F.; Chen, Y.; Gao, W. A novel and sensitive fluorescence sensor for glutathione detection by controlling the surface passivation degree of carbon quantum dots. *Talanta* **2017**, *166*, 1–7. [[CrossRef](#)] [[PubMed](#)]
16. Chen, J.; Huang, Z.; Meng, H.; Zhang, L.; Ji, D.; Liu, J.; Yu, F.; Qu, L.; Li, Z. A facile fluorescence lateral flow biosensor for glutathione detection based on quantum dots-MnO₂ nanocomposites. *Sens. Actuators B Chem.* **2018**, *260*, 770–777.
17. Dai, C.; Yang, C.; Yan, X. Self-quenched gold nanoclusters for turn-on fluorescence imaging of intracellular glutathione. *Nano Res.* **2018**, *11*, 2488–2497. [[CrossRef](#)]
18. Li, Y.; Deng, Y.; Zhou, X.; Hu, J. A label-free turn-on-off fluorescent sensor for the sensitive detection of cysteine via blocking the Ag⁺-enhancing glutathione-capped gold nanoclusters. *Talanta* **2018**, *179*, 742–752. [[CrossRef](#)]
19. Iqbal, A.; Iqbal, K.; Xu, L.; Li, B.; Gong, D.; Liu, X.; Guo, Y.; Liu, W.; Qin, W.; Guo, H. Heterogeneous synthesis of nitrogen-doped carbon dots prepared via anhydrous citric acid and melamine for selective and sensitive turn on-off-on detection of Hg (II), glutathione and its cellular imaging. *Sens. Actuators B Chem.* **2018**, *255*, 1130–1138.
20. Wu, D.; Li, G.; Chen, X.; Qiu, N.; Shi, X.; Chen, G.; Sun, Z.; You, J.; Wu, Y. Fluorometric determination and imaging of glutathione based on a thiol-triggered inner filter effect on the fluorescence of carbon dots. *Microchim. Acta* **2017**, *184*, 1923–1931. [[CrossRef](#)]
21. Gogoi, S.; Khan, R. NIR upconversion characteristics of carbon dots for selective detection of glutathione. *New J. Chem.* **2018**, *42*, 6399–6407. [[CrossRef](#)]
22. Qian, Z.; Ma, J.; Shan, X.; Feng, H.; Shao, L.; Chen, J. Highly luminescent N-doped carbon quantum dots as an effective multifunctional fluorescence sensing platform. *Chem. Eur. J.* **2014**, *20*, 2254–2263. [[CrossRef](#)] [[PubMed](#)]
23. Sheng, Z.; Chen, L. Switch-on fluorescent strategy based on crystal violet-functionalized CdTe quantum dots for detecting L-cysteine and glutathione in water and urine. *Anal. Bioanal. Chem.* **2017**, *409*, 6081–6090. [[CrossRef](#)] [[PubMed](#)]
24. Tian, D.; Qian, Z.; Xia, Y.; Zhu, C. Gold nanocluster-based fluorescent probes for near-infrared and turn-on sensing of glutathione in living cells. *Langmuir* **2012**, *28*, 3945–3951. [[CrossRef](#)] [[PubMed](#)]
25. Gu, W.; Yan, Y.; Cao, X.; Zhang, C.; Ding, C.; Xian, Y. A facile and one-step ethanol-thermal synthesis of MoS₂ quantum dots for two-photon fluorescence imaging. *J. Mater. Chem. B* **2016**, *4*, 27–31. [[CrossRef](#)]
26. Zhao, M.; Chen, A.Y.; Huang, D.; Chai, Y.Q.; Zhuo, Y.; Yuan, R. MoS₂ quantum dots as new electrochemiluminescence emitters for ultrasensitive bioanalysis of lipopolysaccharide. *Anal. Chem.* **2017**, *89*, 8335–8342. [[CrossRef](#)] [[PubMed](#)]
27. Wu, D.; Wang, Y.; Wang, F.; Wang, H.; An, Y.; Gao, Z.; Xu, F.; Jiang, K. Oxygen-incorporated few-layer MoS₂ vertically aligned on three-dimensional graphene matrix for enhanced catalytic performances in quantum dot sensitized solar cells. *Carbon* **2017**, *123*, 756–766. [[CrossRef](#)]
28. Yuan, P.; Walt, D.R. Calculation for fluorescence modulation by absorbing species and its application to measurements using optical fibers. *Anal. Chem.* **1987**, *59*, 2391–2394. [[CrossRef](#)]
29. Shao, N.; Zhang, Y.; Cheung, S.M.; Yang, R.H.; Chan, W.H.; Mo, T.; Li, K.; Liu, F. Copper ion-selective fluorescent sensor based on the inner filter effect using a spiropyran derivative. *Anal. Chem.* **2005**, *77*, 7294–7303. [[CrossRef](#)]
30. Zhai, W.Y.; Wang, C.X.; Yu, P.; Wang, Y.X.; Mao, L.Q. Single-layer MnO₂ nanosheets suppressed fluorescence of 7-hydroxycoumarin: Mechanistic study and application for sensitive sensing of ascorbic acid in vivo. *Anal. Chem.* **2014**, *86*, 12206–12213. [[CrossRef](#)]
31. Liu, J.; Meng, L.; Fei, Z.; Dyson, P.J.; Jing, X.; Liu, X. MnO₂ nanosheets as an artificial enzyme to mimic oxidase for rapid and sensitive detection of glutathione. *Biosens. Bioelectron.* **2017**, *90*, 69–74. [[CrossRef](#)] [[PubMed](#)]
32. Kai, K.; Yoshida, Y.; Kageyama, H.; Saito, G.; Ishigaki, T.; Yu, F.; Kawamata, J. Room-temperature synthesis of manganese oxide monosheets. *J. Am. Chem. Soc.* **2008**, *130*, 15938–15943. [[CrossRef](#)] [[PubMed](#)]
33. Guan, G.J.; Zhang, S.; Liu, S.; Cai, Y.; Low, M.; Teng, C.P.; Phang, I.Y.; Cheng, Y.; Duei, K.L.; Srinivasan, B.M.; et al. Protein induces layer-by-layer exfoliation of transition metal dichalcogenides. *J. Am. Chem. Soc.* **2015**, *137*, 6152–6155. [[CrossRef](#)] [[PubMed](#)]

34. Wang, Y.; Ni, Y. Molybdenum disulfide quantum dots as a photoluminescence sensing platform for 2,4,6-trinitrophenol detection. *Anal. Chem.* **2014**, *86*, 7463–7470. [[CrossRef](#)] [[PubMed](#)]
35. Zhang, X.-L.; Zheng, C.; Guo, S.-S.; Li, J.; Yang, H.-H.; Chen, G. Turn-on fluorescence sensor for intracellular imaging of glutathione using g-C₃N₄ nanosheet–MnO₂ sandwich nanocomposite. *Anal. Chem.* **2014**, *86*, 3426–3434. [[CrossRef](#)] [[PubMed](#)]
36. Deng, R.; Xie, X.; Vendrell, M.; Chang, Y.T.; Liu, X. Intracellular glutathione detection using MnO₂-nanosheet-modified upconversion nanoparticles. *J. Am. Chem. Soc.* **2011**, *133*, 20168–20171. [[CrossRef](#)] [[PubMed](#)]
37. Xu, Y.; Chen, X.; Chai, R.; Xing, C.; Li, H.; Yin, X. A magnetic/fluorometric bimodal sensor based on carbon dots MnO₂ platform for glutathione detection. *Nanoscale* **2016**, *8*, 13414–13421. [[CrossRef](#)]
38. Liu, Z.; Cai, X.; Lin, X.; Zheng, Y.; Wu, Y.; Chen, P.; Weng, S.; Lin, L.; Lin, X. Signal-on fluorescent sensor based on QDs–MnO₂ composite for glutathione. *Anal. Methods* **2016**, *8*, 2366–2374. [[CrossRef](#)]
39. Feng, J.; Huang, P.; Shi, S.; Deng, K.; Wu, F. Colorimetric detection of glutathione in cells based on peroxidase-like activity of gold nanoclusters: A promising powerful tool for identifying cancer cells. *Anal. Chim. Acta* **2017**, *967*, 64–69. [[CrossRef](#)]
40. Wang, Y.; Lu, J.; Tang, L.; Chang, H.; Li, J. Graphene oxide amplified electrogenerated chemiluminescence of quantum dots and its selective sensing for glutathione from thiol-containing compounds. *Anal. Chem.* **2009**, *81*, 9710–9715. [[CrossRef](#)]
41. Michelet, F.; Gueguen, R.; Leroy, P.; Wellman, M.; Nicolas, A.; Siest, G. Blood and plasma glutathione measured in healthy subjects by HPLC: Relation to sex, aging, biological variables, and life habits. *Clin. Chem.* **1995**, *41*, 1509–1517. [[PubMed](#)]
42. Yu, F.; Li, P.; Wang, B.; Han, K. Reversible near-infrared fluorescent probe introducing tellurium to mimetic glutathione peroxidase for monitoring the redox cycles between peroxyxynitrite and glutathione in vivo. *J. Am. Chem. Soc.* **2013**, *135*, 7674–7680. [[CrossRef](#)] [[PubMed](#)]
43. Yuan, Y.; Wu, S.; Shu, F.; Liu, Z. An MnO₂ nanosheet as a label-free nanoplatform for homogeneous biosensing. *Chem. Commun.* **2014**, *50*, 1095–1097. [[CrossRef](#)] [[PubMed](#)]



© 2019 by the authors. Licensee MDPI, Basel, Switzerland. This article is an open access article distributed under the terms and conditions of the Creative Commons Attribution (CC BY) license (<http://creativecommons.org/licenses/by/4.0/>).